Journal of Molecular Spectroscopy **211,** 189–197 (2002)
doi:10.1006/jmsp.2001.8472, available online at http://www.idealibrary.com on IDEAL®

The Bending Vibrational Ladder of $H^{13}C^{15}N$ by Hot Gas Emission Spectroscopy

Wolfgang Quapp,* Vladlen Melnikov,*,[1] and Georg Ch. Mellau†

*Mathematisches Institut, Universität Leipzig, Augustus-Platz, D-04109 Leipzig, Germany; and †Physikalisch-Chemisches Institut, Justus-Liebig-Universität Giessen, Heinrich-Buff-Ring 58, D-35392 Giessen, Germany

Received June 21, 2001; in revised form October 10, 2001

High-resolution measurements have been made on the infrared emission spectrum of the doubly substituted HCN isotopomer, $H^{13}C^{15}N$, at temperatures on the order of 1370 K. The measurements cover the region 400–850 cm^{-1} with a resolution (1/MOPD) of 0.006 cm^{-1}. We could assign hot bands with upper levels up to the $0\ 11^{11}\ 0$ state. The assignments have been verified for states up to $v_2 = 5$ by fitting with earlier room temperature absorption measurements of overtone and hot bands. All the measurements for $H^{13}C^{15}N$ have been combined in a single least-squares fit that includes approximately 8670 rovibrational lines which have a root-mean-square deviation on the order of 0.000 33 cm^{-1}. The spectroscopic constants for the bending states $v_2 = 1, \ldots, 11$ are reported, as well as those for some combination states involving the two stretching modes.

INTRODUCTION

In a recent paper (*1*) we reported the analysis of the high-temperature emission spectrum of $D^{13}C^{15}N$. The present paper is a continuation of that work. The spectrum of hydrogen cyanide, HCN, and those of its isotopomers have been measured extensively (*2–7*) because it is very simple and yet it shows many features that are of interest from a theoretical point of view. The spectrum is also the basis for comparison with *ab initio* calculations (*8*) including theoretical dipole moments and Herman–Wallis coefficients of the HCN isotopomers. The bending mode is of particular interest because of the large-amplitude motion of the proton and also because the bending motion is a direct pathway to the isocyanide isomer, HNC (*9*). In earlier work Maki (*10*) showed that high-temperature absorption measurements of HCN can be used to observe transitions to quite high bending states. In another high-temperature study Maki and Sams (*11*) showed that absorption spectra could be obtained for HNC in equilibrium with HCN.

We have used an isotopically enriched sample of $H^{13}C^{15}N$. This linear molecule has three normal modes, two stretching vibrations of Σ^+ symmetry and the bending mode of Π symmetry: ν_1 is the CH stretch at 3292.29 cm^{-1}, ν_3 is the CN stretch at 2029.63 cm^{-1}, and ν_2 is the degenerate bending mode at 705.01 cm^{-1}. Prior to this work there had been only a few infrared measurements of this twice-substituted species (*4, 12, 13*). The first determination of the ν_1 fundamental wavenumber of this isotopomer was reported by Alpert *et al.* (*12*). The transition to the $v_1 = 2$ band was given by Sasada and Yamada (*13*). The ν_3 fundamental (of all four HCN isotopomers) was the focus of our treatment (*4*). Further Refs. (*14–16*) were microwave or millimeter-wave studies. We have recently reported many new infrared measurements for $H^{12}C^{14}N$, $H^{13}C^{14}N$, and $H^{12}C^{15}N$ (*7*). In that work the vibrational energy levels and rotational constants were fitted to a power series in the vibrational quantum numbers in a parallel fashion for all included isotopomers. In the present work we continue to apply that approach to the isotopomer $H^{13}C^{15}N$. The present work was undertaken to obtain further data for a systematic body of measurements giving an overview of the HCN potential energy surface and the pathway to isomerization.

Using a newly constructed emission apparatus (*1*), we have studied the emission spectrum of the isotopically enriched molecule $H^{13}C^{15}N$ at 1370 K in the range from 400 to 850 cm^{-1}. The emission spectrum yielded many transitions to previously unobserved bending states up to $v_2 = 11$ and some combinations of the CN stretch mode, ν_3, with various quanta of the bending mode, ν_2. Such high bending states can be observed because of the vibrational dependence of the harmonic oscillator transition moment, which has been described by Maki *et al.* (*1, 3*). We also report older room-temperature absorption measurements of this isotopomer of HCN in different wavenumber ranges. So, parallel to the analysis of the $H^{13}C^{15}N$ emission measurements, we have made analyses for room temperature absorption measurements (*2–6*).

Results concerning the emission spectroscopy of the HNC isomer are reported in Ref. (*9*). The present measurement extends our accurate knowledge of the bending potential of the $H^{13}C^{15}N$ isotopomer to levels that are well above the ground

Supplementary data for this article are available on IDEAL (http://www.idealibrary.com) and as part of the Ohio State University Molecular Spectroscopy Archives (http://msa.lib.ohio-state.edu/jmsa_hp.htm).

[1] Permanent address: Laboratory of Molecular Spectroscopy, Physics Department, Tomsk State University, Tomsk 634050, Russia.

0022-2852/02 $35.00

TABLE 1
Parameters of FTS Spectral Emission Measurement

Filename	EDCNECS	EHCNETS
Species	$D^{13}C^{15}N$	$H^{13}C^{15}N$
Region (cm^{-1})	400–877	391–855
Date (D/M/Y)	04/02/1998	30/01/1997
Pressure (mbar)	3.2	3.3
Temperatur (K)	1370	1370
Pathlength (cm) of heated region	60	60
Aperture diameter (mm)	3.15	3.15
Resolution (1/MOPD) (cm^{-1})	0.005	0.006
Bandpass opt. filter (cm^{-1})	400-900(4 K)	400-900(4 K)
High pass el. filter (cm^{-1})	194	194
Low pass el. filter (cm^{-1})	1026	1026
Scans coadded	680	600
Highest S/N (rms)	1000	1000
Detector	Ge : Cu(4 K)	Ge : Cu(4 K)
Windows	KBr	KBr
Beamsplitter	Ge : KBr	Ge : KBr
Focal length collimator (mm)	418	418
Scanner velocity (cm/s)	1.266	1.266

state of the $H^{15}N^{13}C$ isomer. The bending mode may be considered the promoting mode for the isomerization process. However, transitions of the $H^{15}N^{13}C$ isomer could not be detected in the spectra reported, recorded at 1370 K.

EXPERIMENTAL ASPECTS

All measurements were carried out in Giessen with a Bruker IFS 120 HR Fourier transform spectrometer with vacuum transfer optics. The isotopically enriched HCN isotopomer is synthesized by treating isotopically labeled potassium cyanide (CIL, Andover, Massachusetts) with phosphorus pentoxide and H_2O, as has been described elsewhere (*4*). The effective purity of the sample was not very well known since it had been used for other experiments before. The experimental setup was described in Ref. (*1*). Table 1 lists the conditions used in the recording of two emission spectra used in this work. These spectra had a resolution (1/MOPD) of 0.006 cm^{-1} at 1370 K and 700 cm^{-1}. Table 2 gives the vibrational transitions that were included in the least-squares fit used for this work. Most of the absorption measurements were taken from spectra used in our earlier papers (*1–6*).

The emission spectrum was calibrated using $H^{13}C^{15}N$ lines from prior room-temperature absorption spectra. The absolute accuracy of the emission line positions is about ± 0.0002 cm^{-1}. The absolute uncertainty of each band center can be estimated by taking the square root of the sum of the squares of the calibration uncertainty and the statistical uncertainty, which is generally less than the calibration uncertainty. Since the higher vibrational energy levels are determined by summing the band centers for several lower vibrational transitions, most of which come from the same spectrum with the same calibration, the error in the

TABLE 2
Band Centers in Wavenumbers [cm^{-1}] for the Infrared Bands Measured in the Present Analysis of $H^{13}C^{15}N$

transition	ν_c	transition	ν_c	transition	ν_c
$0\,1^1 0\text{-}0\,0^0 0$	705.00445†*	$0\,6^0 0\text{-}0\,5^1 0$	673.47939*	$0\,2^0 1\text{-}0\,1^1 1$	689.53114†*
$0\,2^0 0\text{-}0\,0^0 0$	1397.64481†	$0\,6^2 0\text{-}0\,5^1 0$	688.97375*	$0\,2^2 1\text{-}0\,1^1 1$	704.26650†*
$0\,2^2 0\text{-}0\,0^0 0$	1412.84939†	$0\,6^4 0\text{-}0\,5^3 0$	704.61126*	$0\,3^1 1\text{-}0\,1^1 0$	1381.86369†
$0\,2^0 0\text{-}0\,1^1 0$	692.64036†*	$0\,6^6 0\text{-}0\,5^5 0$	720.34273*	$0\,3^1 1\text{-}0\,2^0 0$	2715.26939†
$0\,2^2 0\text{-}0\,1^1 0$	707.84494†*	$0\,7^1 0\text{-}0\,6^0 0$	676.31352*	$0\,3^1 1\text{-}0\,2^2 0$	2695.85259†
$0\,3^1 0\text{-}0\,0^0 0$	2093.14145†	$0\,7^1 0\text{-}0\,6^2 0$	660.81916*	$0\,3^3 1\text{-}0\,2^2 0$	2736.65386†
$0\,3^3 0\text{-}0\,0^0 0$	2123.64975†	$0\,7^3 0\text{-}0\,6^2 0$	691.99996*	$0\,4^0 1\text{-}0\,2^0 0$	3395.58626†
$0\,3^1 0\text{-}0\,1^1 0$	1388.14367†	$0\,7^5 0\text{-}0\,6^4 0$	707.82852*	$0\,4^2 1\text{-}0\,2^2 0$	3395.30640†
$0\,3^1 0\text{-}0\,2^0 0$	696.90276†*	$0\,7^7 0\text{-}0\,6^6 0$	723.74432*	$1\,0^0 0\text{-}0\,0^0 0$	3292.28515†
$0\,3^1 0\text{-}0\,2^2 0$	680.29206†*	$0\,8^6 0\text{-}0\,7^5 0$	711.13238*	$1\,0^0 0\text{-}0\,1^1 0$	2587.28070†
$0\,3^3 0\text{-}0\,2^2 0$	710.80036†*	$0\,8^8 0\text{-}0\,7^7 0$	727.25354*	$1\,1^1 0\text{-}0\,1^1 0$	3273.56446†
$0\,4^0 0\text{-}0\,0^0 0$	2776.25941†	$0\,9^7 0\text{-}0\,8^6 0$	714.52006*	$1\,1^1 0\text{-}0\,2^0 0$	2580.93313†
$0\,4^0 0\text{-}0\,1^1 0$	2071.25496†	$0\,9^9 0\text{-}0\,8^8 0$	730.86808*	$1\,1^1 0\text{-}0\,2^2 0$	2565.72855†
$0\,4^2 0\text{-}0\,1^1 0$	2086.58146†	$0\,10^8 0\text{-}0\,9^7 0$	717.99285*	$1\,2^0 0\text{-}0\,2^0 0$	3254.79151†
$0\,4^0 0\text{-}0\,3^1 0$	683.11796†*	$0\,10^{10} 0\text{-}0\,9^9 0$	734.58968*	$1\,2^2 0\text{-}0\,2^2 0$	3254.64946†
$0\,4^2 0\text{-}0\,3^1 0$	698.44446†*	$0\,11^{11} 0\text{-}0\,10^{10} 0$	738.42184*	$1\,3^1 0\text{-}0\,3^1 0$	3235.83560†
$0\,4^2 0\text{-}0\,3^3 0$	667.93616†*	$0\,0^0 1\text{-}0\,0^0 0$	2029.63207†	$1\,3^3 0\text{-}0\,3^3 0$	3235.48827†
$0\,4^4 0\text{-}0\,3^3 0$	713.86931†*	$0\,1^1 1\text{-}0\,0^0 0$	2731.05051†	$1\,4^0 0\text{-}0\,4^0 0$	3216.87495†
$0\,5^1 0\text{-}0\,2^0 0$	2064.62693†	$0\,1^1 1\text{-}0\,1^1 0$	2026.04606†	$1\,4^2 0\text{-}0\,4^2 0$	3216.67553†
$0\,5^3 0\text{-}0\,2^2 0$	2080.21962†	$0\,1^1 1\text{-}0\,0^0 1$	701.41844†*	$1\,4^4 0\text{-}0\,4^4 0$	3216.06580†
$0\,5^1 0\text{-}0\,4^0 0$	686.01233*	$0\,2^0 1\text{-}0\,0^0 0$	3420.58165†	$2\,0^0 0\text{-}0\,0^0 0$	6480.58638†
$0\,5^1 0\text{-}0\,4^2 0$	670.68583*	$0\,2^2 1\text{-}0\,0^0 0$	3435.31701†	$1\,0^0 1\text{-}0\,0^0 1$	3279.73220†
$0\,5^3 0\text{-}0\,4^2 0$	701.48310*	$0\,2^0 1\text{-}0\,1^1 0$	2715.57720†	$1\,1^1 1\text{-}0\,1^1 1$	3261.05170†
$0\,5^3 0\text{-}0\,4^4 0$	655.54995*	$0\,2^2 1\text{-}0\,1^1 0$	2730.31256†		
$0\,5^5 0\text{-}0\,4^4 0$	717.05067*				

* indicates the band was measured in emission.
† indicates the band was measured in absorption.

vibrational term values may be more accurately given by the product $v_2 \times (\pm 0.0002)$ cm^{-1}.

For the absorption measurements we used a commercial White-type multipass absorption cell made of borosilicate glass (Infrared Analysis Inc., New York). The cell had a base length of 0.82 m and a volume of approximately 7 L. The optical pathlength was varied between 4 and 24 passes. Sample pressures were restricted to values below 600 Pa to avoid significant pressure-induced line broadening and shift effects. Absorption measurements were made on the isotopically enriched sample of $H^{13}C^{15}N$ from 450 to 800 cm^{-1}, from 1850 to 2400 cm^{-1}, and from 2600 to 3600 cm^{-1}. Bands outside those regions were observed either in the spectrum of $H^{12}C^{15}N$ or in absorption with samples containing $H^{13}C^{14}N$. The former segments were measured with a resolution of 0.003 cm^{-1}, while the latter segment was measured with a resolution of 0.005 cm^{-1}. Most of the strong lines were measured with pressures below 100 Pa but the weakest lines were measured with pressures up to 600 Pa (<5 Torr). For the calibration of the absorption spectra we used wavenumbers of H_2O, CO, OCS, or N_2O lines present in the spectrum (*17*). Since the calibration constants were strongly dependent on the pathlength adjustment of the multipass cell, each run had to be calibrated individually. The tables given in this paper report the statistically determined uncertainty in the band centers. The uncertainty of the absorption measurements due to calibration below and above 1500 cm^{-1} was determined to be ± 0.0002 cm^{-1} and ± 0.0004 cm^{-1}, respectively.

ANALYSIS OF THE MEASUREMENTS

Assignment of the Transitions

In Fig. 1 we present an overview of the quite dense emission spectrum of the v_2 region. The band center of the v_2 fundamental of $H^{13}C^{15}N$ lies at 705.01 cm^{-1}. Figure 2 shows a blow-up of some Q-branches in the v_2 region. The assignment of transitions was aided by the Giessen Loomis–Wood program (*18*). This program cuts the spectrum into segments of $2B$, where B is the rotational constant, and displays schematically consecutive segments, one above the other, on the monitor. With a good estimate of B″ and δB, lines belonging to a single subband will appear aligned in a recognizable pattern. Based on assignments of earlier absorption measurements, it was quite easy to assign emission transitions to levels that had already been observed. A peculiarity of the $H^{13}C^{15}N$ isotopomer is a regular clustering, in this presentation, of the ladder of successive l_{max} hot bands of the bending mode, beginning with $v_2 = 5$. This is analogous to the $D^{13}C^{15}N$ isotopomer; cf. Fig. 2 of Ref. (*1*). The nearly parallel alignment of peaks in the Loomis–Wood screen makes the assignment of higher v_2 states remarkably easy. The nice behavior of such transitions contrasts strongly with transitions between lower l-sublevels, for example, the 4^0, 5^1, 6^0, 6^2, 7^1, and 7^3 states, where the Loomis–Wood-picture is curvilinear and difficult to assign.

Estimated constants from previous data (*7, 14, 16*) or constants determined from a preliminary fit were useful in verifying the assignments. For emission spectra such as these, quite crowded with a high density of lines, one must have a system for verifying new assignments based on predictions. Sometimes it seems we could assign any predicted transition because there is always a line near the predicted position! We have used several criteria for verifying our assignments: intensity, l-resonance splittings, rms-deviation of the fit, and smooth variation of the rovibrational constants with vibrational quantum numbers. From calculated intensities (see Ref. (*1*)) we know approximately how strong each transition should be. If a transition is too strong, it may be overlapped by another transition,

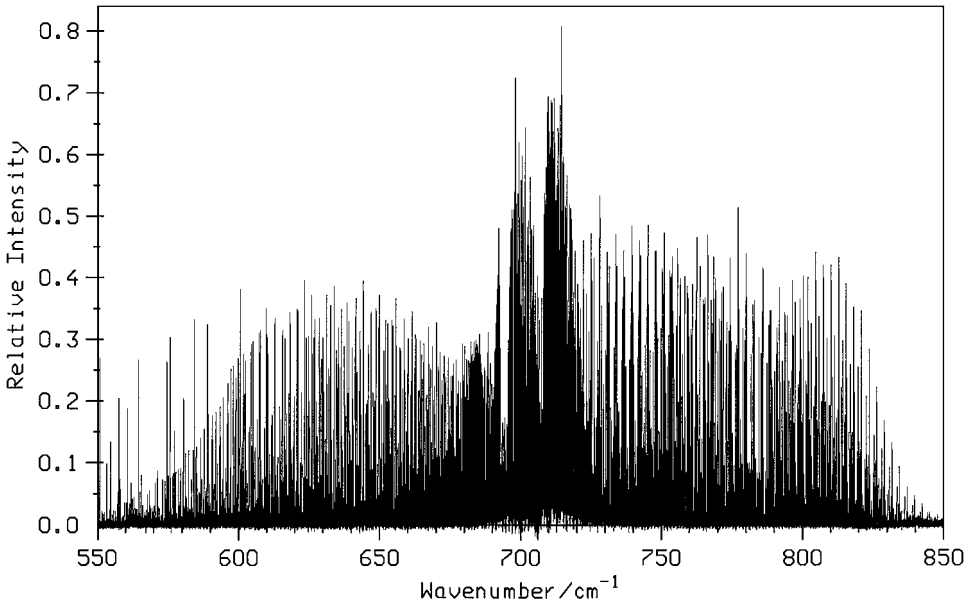

FIG. 1. Overview of the emission spectrum of the v_2 region for $H^{13}C^{15}N$. The band center of the fundamental lies at 705 cm^{-1}.

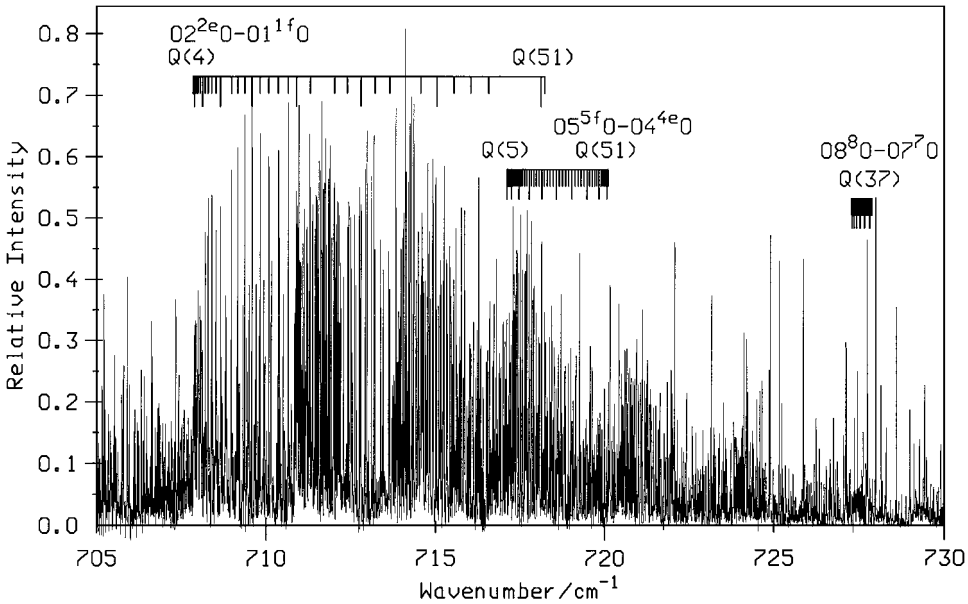

FIG. 2. Part of the emission spectrum with the Q-branches in the ν_2 region of $H^{13}C^{15}N$. The clusters can be assigned to the quantum numbers $v_2 = 2$ through 8. For $v_2 = 2$, 5, and 8 the dominant Q-branch is specifically labeled.

but if it is too weak or is missing, then we must conclude that there is something wrong with our other assignments for the band in question. All transitions used in the fits had relative intensities that were in approximate agreement with the expected band intensity. No evidence was found for perturbations of the bands reported here. In many cases the J and l assignments of $H^{13}C^{15}N$ could be verified by the splitting of the e and f levels, which can be resolved at sufficiently high J values. Even a crude approximation of the value of the l-type resonance constant will give an accurate estimate for the J-value at which the splitting should first be observed for levels with $l > 1$.

As a general rule, we have found that most of the transitions could be fit with an rms deviation of 0.0004 cm^{-1} or better. Weak transitions have somewhat larger rms deviations and some judgment had to be used to estimate what was an acceptable uncertainty for the weakest transitions. Usually, we have excluded those individual lines from the fit which have a deviation of more than ± 0.0012 cm^{-1} from the calculated line position. In many cases a given vibrational state was involved in more than one band. Our fitting procedure combines all the transitions involving a given state to obtain a single set of constants for that state. In Table 2 we give the band centers of the infrared transitions used. Additionally, the band 200–000 is taken from supplementary material of Sasada and Yamada (*13*). In Table 3 we also give the largest J-value, J_{max}, that was included in the least-squares fit of the corresponding state. In addition to the infrared measurements, the known millimeter-wave measurements (*16*) were included in the fit for the states $0\,0^0 0$, $0\,1^1 0$, $0\,2^0 0$, $0\,2^2 0$, and the direct l-type doublets between $0\,1^{1f}0$ and $0\,1^{1e}0$.

Vibrational and Rotational Constants

The constants of $H^{13}C^{15}N$ obtained from the analysis of these measurements are given in Tables 3 to 6. The present analysis is the same as that given in our earlier papers but we give in the tables constants that are based on a more standardized notation. The observed transition wavenumbers, ν_{obs}, were fit with a nonlinear least-squares fitting program for which

$$\nu_{obs} = T(v, l, J)' - T(v, l, J)'' \qquad [1]$$

where the prime ($'$) and double prime ($''$) stand for the respective upper and lower state term values. The term values, $T(v, l, J)$, are given by the appropriate eigenvalues for the matrix formed with the diagonal matrix elements

$$\begin{aligned}\langle v_1, v_2, v_3, l, J\ |\mathbf{H}/hc|v_1, v_2, v_3, l, J\rangle &= G_0(v, l) + B_v[J(J+1) - l^2] - D_v[J(J+1) - l^2]^2 \\ &\quad + H_v[J(J+1) - l^2]^3, \end{aligned} \qquad [2]$$

and with off-diagonal matrix elements

$$\begin{aligned}\langle v_1, v_2, v_3, l, J\ |\mathbf{H}/hc|v_1, v_2, v_3, l \pm 2, J\rangle &= \frac{1}{4}\{q_v - q_{vJ}J(J+1) + q_{vJJ}J^2(J+1)^2 + q_l(l \pm 1)^2\} \\ &\quad \times \{(v_2 \mp l)(v_2 \pm l + 2)[J(J+1) - l(l \pm 1)] \\ &\quad \times [J(J+1) - (l \pm 1)(l \pm 2)]\}^{1/2} \end{aligned} \qquad [3]$$

TABLE 3
Rovibrational Constants in cm^{-1} for $H^{13}C^{15}N$ after Correcting for *l*-Type Resonance

v_1	v_2	l	v_3	$G_0(v,l)$[a]	B_v	$D_v \times 10^6$	$H_v \times 10^{12}$	J_{max}
0	0	0	0	0.00	1.396430982(36)[b]	2.608(8)	2.87(30)	65
0	1	1	0	706.403903(13)	1.399449518(28)	2.66304(8)	3.353 (3)	65
0	2	0	0	1397.644814(18)	1.402930999(69)	2.7188(11)	4.3123(4)	60
0	2	2	0	1418.458050(24)	1.402164591(42)	2.71499(9)	3.4596(3)	60
0	0	0	1	2029.632068(21)	1.38709288(14)	2.61362(23)	2.8858(1)	39
0	3	1	0	2094.547576(20)	1.40612392(10)	2.77239(37)	4.8759(4)	57
0	3	3	0	2136.290719(47)	1.40455227(17)	2.76304(36)	3.1953(6)	64
0	4	0	0	2776.259407(33)	1.40981333(23)	2.82892(73)	6.0578(1)	49
0	4	2	0	2797.221934(30)	1.40900534(12)	2.82316(37)	[5.5375][c]	59
0	4	4	0	2860.024474(71)	1.40658828(25)	2.80628(66)	2.3108(9)	65
0	1	1	1	2732.440527(18)	1.39001279(12)	2.66757(20)	3.4423(9)	52
1	0	0	0	3292.285146(24)	1.38721060(11)	2.58815(14)	3.1772(5)	49
0	2	0	1	3420.581653(27)	1.39336709(15)	2.71692(14)	[4.3424]	46
0	2	2	1	3440.887526(28)	1.39262874(13)	2.71881(11)	[3.6181]	44
0	5	1	0	3463.684953(61)	1.41320943(38)	2.8793(10)	6.0603(3)	54
0	5	3	0	3505.772944(81)	1.41154860(30)	2.87045(34)	[5.7880]	45
0	5	5	0	3589.77590(10)	1.40824691(43)	2.8453(11)	1.8303(2)	55
1	1	1	0	3979.968363(31)	1.39041887(15)	2.64888(21)	4.0971(8)	45
0	3	1	1	4114.310642(35)	1.39644216(23)	2.76966(47)	[5.0556]	34
0	3	3	1	4155.111909(88)	1.39491413(70)	2.7636(11)	[3.6070]	26
1	2	0	0	4652.436318(31)	1.39410836(17)	2.71277(16)	[4.7880]	38
1	2	2	0	4673.072130(35)	1.39332025(11)	2.70439(10)	[4.0637]	42
0	4	0	1	4793.231072(81)	1.39999610(99)	2.8188(17)	[6.2617]	26
0	4	2	1	4813.752607(87)	1.39920534(79)	2.8129(15)	[5.5375]	26
0	4	4	1	[4875.246298]	[1.3968386]	[2.7952]	[3.3646]	—
1	0	0	1	5309.364268(73)	1.37806443(49)	2.60008(61)	[3.3919]	31
0	6	0	0	4135.75113(11)	1.41713958(82)	2.9439(22)	[8.7044]	39
0	6	2	0	4156.91064(11)	1.41628683(59)	2.9246(17)	[7.9801]	43
0	6	4	0	4220.29993(15)	1.41372880(80)	2.91428(94)	[5.8072]	33
0	6	6	0	4325.65456(18)	1.40950300(94)	2.8808(23)	2.2357(7)	39
1	3	1	0	5330.374553(41)	1.39750337(27)	2.76961(54)	[5.5012]	30
1	3	3	0	5371.701063(69)	1.39589363(40)	2.75979(58)	[4.0526]	30
0	7	1	0	4813.48543(17)	1.4207810(18)	2.9761(43)	[9.9409]	29
0	7	3	0	4856.01661(41)	1.4190182(38)	3.0204(96)	[8.4923]	23
0	7	5	0	4940.89655(27)	1.4155104(13)	2.9461(16)	[5.5951]	32
0	7	7	0	5067.76269(23)	1.41032468(93)	2.9071(29)	0.5756(7)	39
1	1	1	1	5993.48340(31)	1.3812002(48)	2.667(13)	[3.8435]	20
1	4	0	0	5993.13436(39)	1.4014058(68)	2.830(22)	[6.7074]	19
1	4	2	0	6013.86379(36)	1.4005896(62)	2.860(23)	[5.9831]	18
1	4	4	0	6075.95470(42)	1.3981157(40)	2.8125(82)	[3.8102]	23
0	8	0	0	[5475.541180]	[1.4249956]	[3.121875]	[10.670]	—
0	8	2	0	[5496.949230]	[1.4240826]	[3.101548]	[10.946]	—
0	8	4	0	[5561.078886]	[1.4213585]	[3.040565]	[8.7732]	—
0	8	6	0	5667.64812(37)	1.4168598(18)	2.9505(20)	[5.1517]	30
0	8	8	0	5816.19411(27)	1.41068425(85)	2.9245(35)	[0.10]	43
0	9	1	0	[6143.117546]	[1.4289058]	[3.188379]	[10.168]	—
0	9	3	0	[6186.197762]	[1.4270258]	[3.146156]	[10.719]	—
0	9	5	0	[6272.164160]	[1.4232952]	[3.061716]	[8.8227]	—
0	9	7	0	6400.63151(57)	1.4177607(25)	2.9687(29)	[4.4769]	32
0	9	9	0	6571.03298(51)	1.4105504(17)	2.9332(48)	[−1.3173]	35
2	0	0	0	6480.58638(24)	1.3777052(24)	2.5619(39)	[3.2]	40
0	10	0	0	[6794.538300]	[1.4333349]	[3.267110]	[10.159]	—
0	10	2	0	[6816.248651]	[1.4324778]	[3.245218]	[10.435]	—

[a] To get the observed band center use

$$G_c(v,l) = G_0(v,l) - B_v l^2 - D_v l^4 - H_v l^6.$$

[b] The uncertainty (one standard deviation) in the last digits is given in parenthesis.
[c] Values enclosed in square brackets were fixed during the fit.

TABLE 3—*Continued*

v_1	v_2	l	v_3	$G_0(v,l)^a$	B_v	$D_v \times 10^6$	$H_v \times 10^{12}$	J_{max}
0	10	4	0	[6881.279641]	[1.4295763]	[3.179540]	[10.262]	—
0	10	6	0	[6989.332916]	[1.4247896]	[3.070078]	[8.6409]	—
0	10	8	0	7139.9160(11)	1.4181559(69)	2.955(12)	3.57087	24
0	10	10	0	7332.35570(88)	1.4098762(34)	2.9163(71)	−2.94777	30
0	11	1	0	[7451.223152]	[1.4376817]	[3.333932]	[10.919]	—
0	11	3	0	[7494.962665]	[1.4356783]	[3.288532]	[10.470]	—
0	11	5	0	[7582.236280]	[1.4317008]	[3.197731]	[10.573]	—
0	11	7	0	[7712.636742]	[1.4258082]	[3.061529]	[8.2278]	—
0	11	9	0	[7885.561938]	[1.4180885]	[2.879927]	[2.4334]	—
0	11	11	0	8100.2259(19)	1.4085617(82)	2.460(15)	−4.8094	26

and

$$\langle v_1, v_2, v_3, l, J \,|\mathbf{H}/hc|v_1, v_2, v_3, l \pm 4, J\rangle = \frac{1}{16}\rho_v\{(v_2 \mp l)(v_2 \pm l + 2)(v_2 \mp l - 2)(v_2 \pm l + 4) \times [J(J+1) - (l \pm 1)]\,[J(J+1) - (l \pm 1)(l \pm 2)] \times [J(J+1) - (l \pm 2)(l \pm 3)][J(J+1) - (l \pm 3) \times (l \pm 4)]\}^{1/2}, \quad [4]$$

where J is the quantum number for overall rotational angular momentum and l is the quantum number for vibrational angular momentum. The matrix has dimensions $(v_2 + 1) \times (v_2 + 1)$. When $v_2 = 0$ this is a 1×1 matrix for which the term value, $T(v, l, J)$, is given by Eq. [2]. The l-type doubling constants are given in Table 4. In our fits we have used the same value of q_l for all values of v_2, cf. Ref. (*7*), which after several cycles was fit at fixed ρ_v values to $q_l = 0.836 \times 10^{-5}$ cm^{-1}, and this value itself was fixed in the final fit. This constant is highly correlated with ρ_v. For vibrationally degenerate states the energy levels are divided into e and f levels defined according to their parity (*19*). For linear triatomic molecules the e levels are below the f levels for all Π and Φ vibrational states while for Δ and Γ states

TABLE 4
l-Type Resonance Constants in cm^{-1} for H^{13}C^{15}N

v_1	v_2	v_3	$q_v \times 10^3$	$q_{vJ} \times 10^8$	$q_{vJJ} \times 10^{12}$	$\rho_v \times 10^8$
0	1	0	6.7498176(66)[a]	7.358(3)	0.97(10)	
0	2	0	6.84591(24)[b]	7.72(1)	1.0(3)	[−1.675][c]
0	3	0	6.945433(56)	8.190(7)	1.2(2)	−1.693(22)
0	4	0	7.04736(10)	8.62(1)	1.3(5)	−1.725(22)
0	1	1	6.73726(14)	7.32(2)	1.0(9)	
0	2	1	6.81354(27)	7.33(1)	[1.10]	[−1.668]
0	5	0	7.15438(10)	9.11(2)	1.2(9)	−1.817(22)
1	1	0	6.889169(78)	8.089(6)	[0.98]	
0	3	1	6.89797(15)	7.91(4)	[1.21]	−1.674(62)
1	2	0	6.99642(30)	8.64(2)	[1.09]	[−1.675]
0	4	1	6.98513(72)	8.12(11)	[1.32]	[−1.792]
0	6	0	7.26138(54)	9.46(4)	[1.55]	−1.685(43)
1	3	0	7.10922(19)	9.11(3)	[1.20]	[−1.737]
0	7	0	7.37894(45)	9.81(12)	[1.67]	−1.730(76)
1	1	1	6.9757(45)	7.0(17)	[0.99]	
1	4	0	7.2220(35)	[9.9]	[1.31]	[−1.800]
0	8	0	[7.4970]	[10.63]	[1.75]	[−2.049]
0	9	0	[7.6210]	[11.17]	[1.87]	[−2.111]
0	10	0	[7.7490]	[11.74]	[1.98]	[−2.174]
0	11	0	[7.8840]	[12.32]	[2.09]	[−2.236]

[a] The uncertainty (one standard deviation) in the last digits is given in parenthesis.
[b] For $v_2 > 1$ the data were fit with $q_l = (0.836 \pm 0.022) \times 10^{-5}$ cm^{-1}.
[c] Values enclosed in square brackets were fixed during the fit.

TABLE 5
Power Series Coefficients for the Vibrational Energy Levels for H^{13}C^{15}N

Coefficient	H^{13}C^{15}N		
ω_1	3422.564 7(37)[a]	z_{1111}	[0.009 67]
ω_2	7194.856 4(49)	z_{2222}	−0.001 081(80)
ω_3	2058.595 5(31)	z_{3333}	[0.005 8]
x_{11}	[−53.292 1][b]	z_{1112}	[−0.017 5]
x_{22}	−2.480 1(26)	z_{1113}	[−0.121]
x_{33}	[−9.6]	z_{1122}	[0.015 5]
x_{12}	−18.221 2(47)	z_{1133}	[0.051 4]
x_{13}	−11.965 7(46)	z_{1123}	[0.093 5]
x_{23}	−3.557 0(34)	z_{1222}	0.003 57(21)
g_{ll}	5.251 6(10)	z_{1333}	[−0.033 6]
y_{111}	[0.37]	z_{1223}	[0.0]
y_{222}	0.018 29(64)	z_{1233}	[0.0]
y_{333}	[−0.039]	z_{2223}	−0.006 86(11)
y_{112}	[−0.083]	z_{2233}	[0.008 26]
y_{122}	−0.114 9(16)	z_{2333}	[−0.002 5]
y_{113}	[−0.29]	z_{11ll}	[−0.018 7]
y_{133}	[0.158]	z_{22ll}	0.001 230(83)
y_{123}	−0.213 3(42)	z_{33ll}	[−0.007 3]
y_{233}	[−0.111]	z_{12ll}	−0.007 85(18)
y_{223}	0.136 41(97)	z_{13ll}	[0.057 4]
y_{1ll}	−0.003 28(68)	z_{23ll}	0.008 78(17)
y_{2ll}	0.004 21(46)	z_{llll}	−0.000 196(18)
y_{3ll}	−0.001 57(61)	z_{2llll}	−0.000 007 7(23)
		z_{222ll}	0.000 014 7(58)
# weighted states in fit:		z_{22222}	−0.000 007 5(40)
	45	SD of Fit	13.2

[a] The uncertainty (one standard deviation) in the last digits is given in parenthesis.
[b] Values enclosed in square brackets were fixed during the fit.

TABLE 6
Power Series Coefficients for the Rovibrational Constants and *l*-Type Resonance Constants in cm^{-1} for $H^{13}C^{15}N$

Coefficient		Coefficient		Coefficient	
$\times 10^3$		$D_e \times 10^6$	2.562 5(3)	$q_e \times 10^3$	6.509 6(10)
B_e	1402.549 561(16)[a]	$\beta_1 \times 10^8$	−2.99(17)	$q_1 \times 10^3$	0.099(11)
α_1	−9.210(11)	$\beta_2 \times 10^8$	5.442(79)	$q_2 \times 10^3$	0.092(3)
α_2	3.042(6)	$\beta_3 \times 10^8$	0.71(20)	$q_3 \times 10^3$	−0.028(11)
α_3	−9.268(11)	$\beta_{11} \times 10^9$	[0.0]	$q_{11} \times 10^4$	[−0.17]
γ_{11}	[−0.137][b]	$\beta_{22} \times 10^9$	−0.145(95)	$q_{22} \times 10^4$	0.012(7)
γ_{22}	0.040 7(14)	$\beta_{33} \times 10^9$	[0.0]	$q_{33} \times 10^4$	[0.0]
γ_{33}	[−0.028]	$\beta_{12} \times 10^9$	6.78(45)	$q_{12} \times 10^4$	0.122(5)
γ_{12}	0.169(11)	$\beta_{13} \times 10^9$	5.8(25)	$q_{13} \times 10^4$	0.99(22)
γ_{13}	−0.156(21)	$\beta_{23} \times 10^9$	−3.90(49)	$q_{23} \times 10^4$	−0.173(5)
γ_{23}	−0.099(12)	$\beta_{ll} \times 10^9$	−0.58(30)	$q_{222} \times 10^4$	−0.000 4(5)
γ_{ll}	−0.181 3(8)	$\beta_{1ll} \times 10^9$	−0.95(19)	SD of Fit	5.0
γ_{111}	[−0.001 5]	$\beta_{2ll} \times 10^9$	−0.18(3)	# weighted states	
γ_{222}	0.000 7 1(21)	$\beta_{3ll} \times 10^9$	1.32(19)		18
γ_{333}	[0.0]	SD of Fit	3.9		
γ_{112}	[0.0]	# weighted states			
γ_{113}	[−0.002 5]		44		
γ_{122}	−0.003 5(3)			$q_{eJ} \times 10^8$	6.31(4)
γ_{223}	−0.009(2)	$H_e \times 10^{12}$	1.999(59)	$q_{1J} \times 10^8$	0.38(3)
γ_{133}	[0.0]	$\epsilon_1 \times 10^{12}$	0.43(11)	$q_{2J} \times 10^8$	0.43(7)
γ_{233}	[0.0]	$\epsilon_2 \times 10^{12}$	0.63(10)	$q_{3J} \times 10^8$	[−0.087]
γ_{123}	0.030(21)	$\epsilon_3 \times 10^{12}$	[0.0]	$q_{11J} \times 10^8$	[0.0]
γ_{1ll}	0.005 2(2)	$\epsilon_{22} \times 10^{12}$	0.023(19)	$q_{22J} \times 10^8$	0.007(8)
γ_{2ll}	−0.003 5(2)	$\epsilon_{ll} \times 10^{12}$	−0.210(11)	$q_{33J} \times 10^8$	[0.0]
γ_{3ll}	−0.013 4(13)	SD of Fit	2.2	$q_{12J} \times 10^8$	[0.057]
γ_{2222}	0.000 014(11)	# weighted states		$q_{13J} \times 10^8$	[0.49]
γ_{2223}	0.000 6 5(24)		18	$q_{23J} \times 10^8$	−0.17(2)
γ_{11ll}	[0.001]			SD of Fit	4.4
γ_{22ll}	−0.000 1 49(15)			# weighted states	
γ_{13ll}	[−0.003 9]	$\rho^* \times 10^8$	−1.439(7)		14
γ_{23ll}	−0.001 48(40)	$\rho_2 \times 10^8$	−0.062(17)	$q^*_{JJ} \times 10^{12}$	0.73(4)
γ_{llll}	0.000 070(5)	$\rho_3 \times 10^8$	0.009(72)	$q_{2JJ} \times 10^{12}$	0.11(2)
SD of Fit	4.3	SD of Fit	1.1	$q_{3JJ} \times 10^{12}$	0.03(20)
# weighted states in fit		# weighted states		SD of Fit	2.3
	46		4	# weighted states	
					4

[a] The uncertainty (one standard deviation) in the last digits is given in parenthesis.
[b] Values enclosed in square brackets were fixed during the fit.

the f levels are below the e levels. We have assigned a positive sign to the q_v constants (*20*) while the signs of the remaining terms in Eqs. [3] and [4] are then determined from the fit of the measurements.

The off-diagonal matrix elements given by Eqs. [3] and [4] represent the effect of l-type resonance, a type of Coriolis resonance. As long as there are no vibrational resonances, the usual definition of the band center of a vibrational transition, ν_c, is given by

$$\nu_c = G_c(v, l)' - G_c(v, l)'', \qquad [5]$$

where

$$G_c(v, l) = G_0(v, l) - B_v l^2 - D_v l^4 - H_v l^6 \quad \text{with } G_0(0, 0) = 0. \qquad [6]$$

The band centers, ν_c, for the bands measured in this work are given in Table 2. The vibrational term values $G_0(v, l)$ are given in Table 3. The least-squares programs used to obtain the constants in Tables 3 to 6 are the same programs used for Refs. (*1–7*).

In only a few cases were all the higher order rovibrational constants adequately determined by the measurements. Rather than arbitrarily set to zero all those constants that could not be determined, we estimated the approximate value of the constants through the series of corresponding H_v, q_{vJJ}, or ρ_v terms. This was carried out by fitting the various constants to a power series in the vibrational quantum numbers as indicated later and extrapolating to estimate the values of those constants that could not be determined because the data were too sparse or too inaccurate. The analysis was done in several cycles. The first cycle determined which constants were determinable from the data. Those

constants were then fit to a power series in order to calculate the undetermined constants for the next cycle. Some constants which could not be determined from the measurements were then held fixed at the calculated values in the next fit of the measurements. This gave improved values for the determinable constants and the cycle was repeated. This self-consistent procedure converged quite rapidly to give the constants reported in Tables 3–6. At the end, we could fit 197 constants of 46 observed rovibrational states, while 142 additional constants of these states, and of 16 other predicted states where fixed to, as we believe, adequate values. The body of data is 10 150 lines, where 8 669 lines in the file are given a weight, and thus were used in the last least-squares fit. All line positions are available as supplementary data.

Vibrational Quantum Number Expansions

The constants given in Tables 5 and 6 were fit to the usual power series expansion in the vibrational quantum numbers v and l to determine a set of constants which could be used to predict further rovibrational constants and unobserved term values. We have successfully used such predicted constants to climb up the bending vibrational ladder of $H^{13}C^{15}N$. The constants allowed us to calculate the emission lines for new vibrational transitions with an accuracy of ± 0.05 cm^{-1} (10 linewidths) or better when extrapolating to the next higher level. For the vibrational constants given in Table 5, we used the expansion

$$\begin{aligned} G_0(v,l) + G(0,0) &= \sum_i^3 \omega_i (v_i + d_i/2) + \sum_{i\le j}^3 x_{ij}(v_i + d_i/2)(v_j + d_j/2) + g_{22} l^2 \\ &+ \sum_{i\le j\le k}^3 y_{ijk}(v_i + d_i/2)(v_j + d_j/2)(v_k + d_k/2) \\ &+ \sum_i^3 y_{ill}(v_i + d_i/2) l^2 + \sum_{i\le j\le k\le h}^3 z_{ijkh}(v_i + d_i/2) \\ &\times (v_j + d_j/2)(v_k + d_k/2)(v_h + d_h/2) \\ &+ \sum_{i\le j}^3 z_{ijll}(v_i + d_i/2)(v_j + d_j/2) l^2 + z_{llll} l^4 \\ &+ z_{222ll}(v_2+1)^3 l^2 + z_{22222}(v_2+1)^5. \end{aligned} \quad [7]$$

Here we use $G_0(0,0) = 0$, then G(0, 0) on the left hand side represents the zero-point vibrational energy. In this and the following equations the sums are over all values of the subscript from 1 to 3 for the three normal modes with $h \ge k \ge j \ge i$. The vibrational degeneracy is given by $d_1 = d_3 = 1$ and $d_2 = 2$.

Since the emission measurements for $H^{13}C^{15}N$ go to very high bending states, it was necessary to include constants in Eq. [7] that involve high powers in the bending quantum number as well as high powers for the quantum number of the vibrational angular momentum, l. The constants are comparable with the higher order terms of the same values for the other isotopomers of HCN (*7*). It is obvious that they only differ by a small amount. In those cases where a constant could not be determined for any isotopomer, it was necessary to set it to zero in the least-squares fit. Nakagawa and Morino (*21*) have given calculated values for the x_{ij} constants for $H^{12}C^{14}N$, $H^{13}C^{14}N$, $H^{12}C^{15}N$, and $H^{13}C^{15}N$ and the ratios of those constants are very close to the ratios we observe. Consequently, we have used their calculated ratios to estimate the isotope shifts in those cases where the constants could not be determined from the measurements made at this time. Strey and Mills (*22*) have also given calculated values for the x_{ij} constants. Although they give fewer significant figures, their values are in fair agreement with those of Nakagawa and Morino.

The rotational constants are fit to

$$\begin{aligned} B_v = B_e &- \sum \alpha_i (v_i + d_i/2) + \sum \gamma_{ij}(v_i + d_i/2)(v_j + d_j/2) \\ &+ \gamma_{ll} l^2 + \sum \gamma_{ijk}(v_i + d_i/2)(v_j + d_j/2)(v_k + d_k/2) \\ &+ \sum \gamma_{ill}(v_i + d_i/2) l^2 + \gamma_{2222}(v_2+1)^4 + \gamma_{2223}(v_2+1)^3 \\ &\times (v_3 + 1/2) + \gamma_{11ll}(v_1 + 1/2)^2 l^2 + \gamma_{22ll}(v_2+1)^2 l^2 \\ &+ \gamma_{13ll}(v_1 + 1/2)(v_3 + 1/2) l^2 + \gamma_{23ll}(v_2+1) \\ &\times (v_3 + 1/2) l^2 + \gamma_{llll} l^4. \end{aligned} \quad [8]$$

The constants on the right hand side of Eq. [8] are given in Table 6. In several cases certain constants could be determined for some other isotopomers. In those cases the constants were set equal to the value found for another isotopomer. When a constant could not be determined for any isotopomer, it was set to zero. The centrifugal distortion constants given in Table 6 were calculated by

$$\begin{aligned} D_v = D_e &+ \sum \beta_i (v_i + d_i/2) + \sum \beta_{ij}(v_i + d_i/2)(v_j + d_j/2) \\ &+ \beta_{ll} l^2 + \sum \beta_{ill}(v_i + d_i/2) l^2 \end{aligned} \quad [9]$$

and

$$H_v = H_e + \sum \epsilon_i (v_i + d_i/2) + \epsilon_{22}(v_2+1)^2 + \epsilon_{ll} l^2. \quad [10]$$

For H_v, the constant ϵ_3 for the stretching mode v_3 could not be estimated; it was set to zero. Note that the quartic centrifugal distortion constant D_e of $H^{13}C^{15}N$ was predicted to 76.79 kHz in an early quantum chemical calculation (*23*), which we can confirm with our measurement. The l-type resonance constants given in Table 6 were fit to the equation

$$\begin{aligned} q_v = q_e &+ \sum q_i (v_i + d_i/2) + \sum q_{ij}(v_i + d_i/2) \\ &\times (v_j + d_j/2) + q_{222}(v_2+1)^3. \end{aligned} \quad [11]$$

The associated J-dependent terms are defined by the expression

$$q_{vJ} = q_{eJ} + \sum q_{iJ}(v_i + d_i/2) + \sum q_{ijJ}(v_i + d_i/2) \times (v_j + d_j/2). \quad [12]$$

Table 6 gives these higher order constants determined for the isotopomer $H^{13}C^{15}N$. As can be seen, there were very few determinable values of q_{vJJ} and ρ_v. Those constants were therefore fit to an abbreviated power series,

$$q_{vJJ} = q^*_{JJ} + q_{2JJ}(v_2 + 1) + q_{3JJ}(v_3 + 1/2) \quad [13]$$

and

$$\rho_v = \rho^* + \rho_{2JJ}(v_2 + 1) + \rho_{3JJ}(v_3 + 1/2). \quad [14]$$

CONCLUSIONS

The constants given in Tables 3 to 6 are in good agreement with those given in our former paper (*7*) and also by the force field calculations of Nakagawa and Morino (*21*) and Strey and Mills (*22*). The current best estimate of the value of B_0 for $H^{13}C^{15}N$, 1.396 430 982(36) cm^{-1}, is comparable with the value given by Preusser and Maki (*16*), 1.396 430 93(14) cm^{-1} within twice its standard deviation.

It is interesting to note that the bending vibration of $H^{13}C^{15}N$ is not very anharmonic. The 11 constants of Table 5 are enough to fit the 26 observed bending levels that extend up to $v_2 = 11$ fairly well. It was earlier found that one almost needed a new constant to fit each measurement of a new stretching state for HCN. This work also demonstrates that emission measurements can be used to explore the ladder of bending vibrational states up to term values of 8100 cm^{-1}, much higher than the ground state of the isocyanide isomer, HNC. The high v_2-states reached in this measurement, as well as in our recent papers (*1, 7*), are approximately half way to the lowest energy-delocalized state crossing the saddle point of the isomerization pathway to $H^{15}N^{13}C$. This level was predicted recently by theoretical treatments (*24*), also see (*25, 26*). On the other hand, on the side of the HNC "bowl" of the potential energy surface, there are states populated up to $v_2 = 5$ at a temperature of 1423 K (*9*). In the data from the present measurement at 1370 K, we could not assign transitions of the heavier isomer $H^{15}N^{13}C$.

Because of the many new measurements of the isotopomer, we can confirm the assignments of the millimeter-wave spectrum given for $v_2 \leq 2$ by Preusser and Maki (*16*). Their measurements as well as all other available data were included in our fit. All of the data of $H^{13}C^{15}N$ that were used in our fits are available as supplementary data.

ACKNOWLEDGMENTS

We are very grateful to Arthur Maki for his continuous and unselfish help for this work. We also thank Manfred and Brenda P. Winnewisser for helpful discussions and valuable comments to the work. V.M. give thanks for a stipend of the Saxon State Ministry of Science and Art. Financial support of the Deutsche Forschungsgemeinschaft is gratefully acknowledged.

REFERENCES

1. W. Quapp, M. Hirsch, G. Ch. Mellau, S. Klee, M. Winnewisser, and A. Maki, *J. Mol. Spectrosc.* **195,** 284–298 (1999).
2. W. Quapp, S. Klee, G. Ch. Mellau, S. Albert, and A. Maki, *J. Mol. Spectrosc.* **167,** 375–382 (1994).
3. A. Maki, W. Quapp, and S. Klee, *J. Mol. Spectrosc.* **171,** 420–434 (1995).
4. A. Maki, W. Quapp, S. Klee, G. Ch. Mellau, and S. Albert, *J. Mol. Spectrosc.* **174,** 365–378 (1995).
5. A. Maki, W. Quapp, S. Klee, G. Ch. Mellau, and S. Albert, *J. Mol. Spectrosc.* **180,** 323–336 (1996).
6. A. Maki, W. Quapp, S. Klee, G. Ch. Mellau, and S. Albert, *J. Mol. Spectrosc.* **185,** 356–369 (1997).
7. A. Maki, G. Ch. Mellau, S. Klee, M. Winnewisser, and W. Quapp, *J. Mol. Spectrosc.* **202,** 67–82 (2000).
8. P. Botschwina, M. Horn, M. Matuschewski, E. Schick, and P. Sebald, *THEOCHEM* **400,** 119–137 (1997).
9. A. G. Maki and G. Ch. Mellau, *J. Mol. Spectrosc.* **209,** 47–52 (2001), doi:10.1006/jmsp.2000.8279.
10. A. G. Maki, *J. Mol. Spectrosc.* **58,** 308–315 (1975).
11. A. G. Maki and R. L. Sams, *J. Chem. Phys.* **75,** 4178–4182 (1981).
12. B. D. Alpert, A. W. Mantz, and K. Narahari Rao, *J. Mol. Spectrosc.* **39,** 159–162 (1971).
13. H. Sasada and K. Yamada, *Appl. Optics* **29,** 3535–3547 (1989), and supplementary data.
14. E. F. Pearson, R. A. Creswell, M. Winnewisser, and G. Winnewisser, *Z. Naturforsch. A* **31,** 1394–1397 (1976).
15. M. Winnewisser and J. Voigt, *Z. Naturforsch. A* **33,** 1323–1327 (1978).
16. J. Preusser and A. G. Maki, *J. Mol. Spectrosc.* **162,** 484–497 (1993).
17. G. Guelachvili and K. Narahari Rao, "Handbook of Infrared Standards." Academic Press, London, 1986.
18. B. P. Winnewisser, J. Reinstädtler, K. M. T. Yamada, and J. Behrend, *J. Mol. Spectrosc.* **136,** 12–16 (1989); F. Stroh, J. Reinstädtler, J. C. Grecu, and S. Albert, "The Giessen Loomis–Wood Program LW 5.1" Justus-Liebig-Universität Giessen, 1992.
19. J. M. Brown, J. T. Hougen, K.-P. Huber, J. W. C. Johns, I. Kopp, H. Lefebvre-Brion, A. J. Merer, D. A. Ramsay, J. Rostas, and R. N. Zare, *J. Mol. Spectrosc.* **55,** 500–503 (1975).
20. K. Yamada, *Z. Naturforsch. A* **38,** 821–834 (1983).
21. T. Nakagawa and Y. Morino, *J. Chem. Soc. Jpn.* **42,** 2212–2219 (1969).
22. G. Strey and I. M. Mills, *Mol. Phys.* **26,** 129–138 (1973).
23. P. Botschwina, *Chem. Phys.* **68,** 41–63 (1982).
24. K. M. Christoffel and J. M. Bowman, *J. Chem. Phys.* **112,** 4496–4505 (2000).
25. W. Jakubetz and B. L. Lan, *Chem. Phys.* **217,** 375–388 (1997).
26. G. J. Harris, O. L. Polyansky, and J. Tennyson, *Spectrochimica Acta A* **58,** 673–690 (2002).